Acta Crystallographica Section D
Biological Crystallography
ISSN 0907-4449

Bence Jones KWR protein structures determined by X-ray crystallography

Debora L. Makino, Agnes H. Henschen-Edman, Steven B. Larson and Alexander McPherson*

University of California, Irvine, Department of Molecular Biology and Biochemistry, Irvine, CA 92697-3900, USA

Correspondence e-mail: amcphers@uci.edu

Received 5 October 2006
Accepted 3 May 2007

PDB References: Bence Jones KWR protein, $P3_121$, 2omb, r2ombsf; $P3_221$, 2old, r2oldsf; $P4_32_12$, 2omn, r2omnsf.

A Bence Jones protein isolated in the early 1960s from a patient (initials KWR) suffering from plasma-cell dyscrasia was crystallized and its structure was analyzed in four different unit cells by X-ray diffraction. The final models of the molecule in all crystal forms were virtually the same, although the elbow angles relating the constant and variable domains of the Bence Jones dimers varied over a range of 10°. The tetragonal form had an R factor of 22.6% and an $R_{\rm free}$ of 28.3% at 2.2 Å resolution. Phosphate or sulfate ions (depending on the crystallization conditions) were found in the antigen-combining sites in all crystals, as well as an unidentified ligand tightly bound in the hydrophobic 'deep pocket' beneath the antigen-binding site. The ligand was treated as a phenol molecule. Two trigonal crystal forms were among those solved. One was grown at pH 4.0 and the other was only obtained after sitting for more than eight months at room temperature. The latter crystal was composed of molecules that were degraded in their constant domains. Both low pH and proteolytic degradation of constant domains are known to promote the polymerization of some Bence Jones proteins into amyloid fibrils. Indeed, in both trigonal crystal forms the molecules are organized with pseudo-hexagonal symmetry about the unique crystallographic axes in a manner suggestive of such fibrils. The arrangement of Bence Jones dimers is also consistent with other observations regarding Bence Jones amyloid-fibril structure and current models.

1. Introduction

In patients with multiple myeloma, a cancer of the bone marrow, clonal proliferation of monoclonal plasma cells results in the excessive production of immunoglobulin light chains, which are termed Bence Jones (BJ) proteins (Clamp, 1967). The proteins are excreted in the patient's urine and in some cases can subsequently be deposited in various tissues (Sanders, 1994). In the former case, they can be recovered and purified in large amounts. BJ proteins are clinically taken to be a first indication of the presence of a tumor and the amount of BJ protein in the urine provides a quantitative measure of the extent of the tumor and the type of proteinuria (Levinson & Keren, 1994). BJ protein is therefore used by physicians not only to diagnose but also to monitor the response of a patient to treatment.

In those cases where the BJ protein is deposited, the protein is frequently found to have suffered some degree of proteolytic degradation and as a consequence forms helical amyloid fibrils (Glenner, 1980), the structures of which have not yet been defined in detail. The formation of such fibrils, their structural features and the way in which they condense to create ordered arrays has assumed increasing importance

because of the similar involvement of protein fibrils in Alzheimer's disease, Down's syndrome, type II diabetes and other diseases (Stone, 1990; Buxbaum, 1992). Owing to their architectural properties, amyloid fibrils have also been used as a model system in nanotechnology applications (Wetzel, 2002; Stevens & Myatt, 1991), as well as a potential target for drug design (Caputo & Salama, 1989).

Bence Jones polypeptides typically have molecular weights of 22 000–24 000 Da and may be characterized as λ or κ chains (Solomon, 1986). The individual immunoglobulin light chains are composed of two domains, either three- or four-stranded or four- or five-stranded β-sheet structures, one of which is constant among different molecules and is called the constant domain and the other of which is variable in amino-acid composition and is referred to as the variable domain. Two light chains associate to form homodimers that are coupled primarily through noncovalent interactions, much as are the light and heavy polypeptide chains comprising the Fab domains of intact antibodies, to which they bear some resemblance. The dimer is further maintained by a disulfide bond between cysteines located in the C-terminal region. A single BJ light-chain variable region displays three characteristic complementarity-determining hypervariable loops (termed CDRs) appropriate for binding a particular antigen, which of course is generally not known. The remainder of the protein exhibits the sequence characteristics of the framework portion of the immunoglobulin light chain.

The two light chains composing a BJ protein dimer thus exist as two constant domains arising from framework residues and two variable domains composed of both framework and CDR residues. The latter domains display two identical sets of three hypervariable loops, which form a quasi antigen-binding site very similar to that of a conventional Fab fragment. Variation among BJ proteins arises not only from amino-acid differences but also from differences between the relative orientations of the pairs of constant and pairs of variable domains and this is characterized by an elbow angle. This angle may vary even among members of a single BJ population. A number of BJ protein structures have been determined using X-ray crystallography, each unique in sequence, antigen specificity, domain dispositions and other detailed features (Epp *et al.*, 1975; Furey *et al.*, 1983; Ely *et al.*, 1989; Huang *et al.*, 1994; Huang, Ainsworth, Solomon *et al.*, 1996; Huang, Ainsworth, Stevens *et al.*, 1996; Roussel *et al.*, 1999; Terzyan *et al.*, 2003).

The BJ protein studied here was purified in gram quantities from the urine of a multiple myeloma patient of initials KWR in Melbourne, Australia in 1962 and stored as a lyophilized powder at room temperature for 40 years before its crystallization for X-ray diffraction analysis was attempted. Biochemical analyses showed the protein not to be degraded or significantly aggregated and to exhibit the normal properties and expected molecular weight of other BJ proteins. The sequence, which is reported here along with its three-dimensional structure, was determined by traditional protein-sequencing methods and shown to be derived from an immunoglobulin λ light chain of subgroup II.

In a previous report (Makino *et al.*, 2005), we described the crystallization of BJ KWR in four different crystal forms and our initial steps to determine the structure of the protein in each. Here, we describe the results of the crystallographic analyses and the refinement of the protein structure in each crystal form. We find interesting certain features of the structure, particularly the manner in which the protein molecules are packed in different forms. In two closely related trigonal crystal forms, the BJ molecules assume a helical pseudo-hexagonal arrangement involving 12 protein dimers about a threefold screw axis. One of these crystal forms is composed of proteolytically degraded molecules and the second was grown at low pH, both of which are circumstances that promote amyloid-fibril formation. The helical arrangement is rather similar to proposed structures for the helical fibril present in BJ deposition diseases. Molecules in the other two crystal forms pack in distinctly different arrangements. In addition, in the trigonal crystals of the BJ protein an intermolecular hydrogen-bonding motif is formed between neighboring dimers, which is consistent with what is known to be a characteristic feature of amyloid-fibril structures (Glenner, 1980). This interaction is not present in the other crystal forms.

2. Experimental procedures

The amino-acid sequence of BJ protein KWR was determined by now conventional protein-sequencing methods (Kintner & Sherman, 2000) that have been described in detail previously (Lounes *et al.*, 2001). Cyanogen bromide fragments were prepared and fractionated on a Sephadex G-50SF column in 0.2% trifluoroacetic acid and quantitative amino-terminal amino-acid sequence analysis was performed with a Hewlett–Packard G1005A protein sequencer (Krieglestein *et al.*, 1990; Lottspeich & Henschen, 1977). Pooled fractions of the fragments were subjected to trypsin digestion for 20 h at room temperature at an estimated 1:50(*w*:*w*) enzyme:substrate ratio. The products were then subjected to mass-spectrometric analysis in a Perceptive Voyager DE Pro matrix-assisted laser desorption/ionization–time of flight (MALDI–TOF) instrument using an α-cyano-4-hydroxycinnamic acid matrix.

As described previously (Makino *et al.*, 2005), four crystal forms of BJ KWR were grown, three from ammonium sulfate, initially at pH 7.0–8.5, and one from sodium/potassium phosphate at pH 3.8–4.2. The crystals were all grown at room temperature by vapor diffusion in Cryschem plates (Hampton Research, Laguna Niguel, CA, USA). The crystals belonged to the tetragonal space group $P4_32_12$ (unit-cell parameters $a = b = 68.6$, $c = 181.7$ Å), the orthorhombic space group $P2_12_12_1$ ($a = 67.7$, $b = 69.4$, $c = 87.3$ Å) and the trigonal space groups $P3_221$ ($a = b = 155.4$, $c = 46.9$ Å) and $P3_121$ ($a = b = 153.5$, $c = 94.0$ Å). The first three crystal forms listed contained one BJ homodimer per asymmetric unit, while the final form listed contained two. The $P3_221$ crystal was the only form obtained at acidic pH. The ambiguity between space group $P4_122$ and $P4_322$ for the tetragonal crystal was, as reported elsewhere, resolved through an atomic force microscopy investigation of the crystals (Plomp *et al.*, 2003). As described further in §3, an

ambiguity arose in the analysis of the crystals of space group $P3_221$, since we assumed that the space group was the same as the first trigonal crystal, space group $P3_121$, which has the same *a*- and *b*-axis length but twice the *c*-axis length. This incorrect space-group assignment also led us to report the likelihood of twinning for the trigonal crystal of shorter *c*-axis length (Makino *et al.*, 2005). This was incorrect, as the crystal is completely ordered and there is no twinning.

The appearance of one of the crystal forms, that of space group $P3_121$, was an irreproducible occurrence. Those crystals were only discovered after more than eight months of standing at room temperature under conditions that normally yielded only the tetragonal and orthorhombic crystal forms. It was immediately recognized therefore that the protein may have been proteolytically degraded to some extent before incorporation into the crystals (McPherson, 1999; McPherson *et al.*, 2004). Unfortunately, there was insufficient crystalline material present in the drop after use for data collection to assess this assumption biochemically. Proteolysis, as described below, was evident from the electron-density maps derived from these crystals.

Data were collected from the tetragonal, orthorhombic and $P3_221$ crystals on beamline 5.0.2 at the Advanced Light Source using flash-frozen specimens. The data for the $P3_121$ crystals were collected at beamline 7-1 at the Stanford Synchrotron Radiation Laboratory. The data were processed using both *HKL*-2000 (Otwinowski & Minor, 1997) and *d*TREK* (Pflugrath, 1999). The relevant statistics for the data sets can be found in our preliminary report (Makino *et al.*, 2005).

The structures of all the crystals were solved using molecular replacement (Rossmann, 1990). A search of the BJ protein entries in the RCSB database (Berman *et al.*, 2000) showed that the amyloidogenic BJ protein MCG, another λ II light-chain dimer formerly thought to be a lambda V (Ely *et al.*, 1989; Bourne *et al.*, 2002), was 87% identical in sequence to BJ KWR. Sequence identity was determined using the program *MULTALIGN* (Barton, 1990) and the Blosum62 comparison table (Henikoff & Henikoff, 1992). This was therefore chosen as the initial search model. The significant structural differences between MCG and KWR were likely to be in the hypervariable loops and the elbow angles between the constant and variable domains. Incremental variation of the unknown elbow angle on the search model was carried out using the program *X-PLOR* (Brünger, 1992) and this was followed by cross-rotation search and translation functions in *CNS* v.1.1 (Brünger *et al.*, 1998), which allowed Patterson correlation refinement of the variable and constant domains as independent groups prior to the translation search. The model derived from the first BJ KWR crystal structure to be solved, that from the $P3_121$ crystals, was then used as the search model for the tetragonal crystal form. The model obtained from the tetragonal crystal form was in turn used to obtain molecular-replacement solutions for the orthorhombic and second trigonal form. For these latter searches, the program *Phaser* (Read, 2001; Storoni *et al.*, 2004) from the *CCP*4 program suite (Collaborative Computational Project, Number 4, 1994) was employed. For the $P3_121$ crystal form, self-rotation functions and native Patterson maps were calculated using *CNS*.

Rigid-body refinements of initial solutions, using the constant and variable domains as independent rigid groups, were carried out at different resolutions to ensure the accuracy of the elbow angles. Refinement by simulated annealing and Powell minimization of all atoms with individual isotropic *B*-factor refinement were carried out using a bulk-solvent correction. Maximum-likelihood targets using structure amplitudes were used in refinement procedures. Water molecules and ions were only added at the end of refinement. The models were built and adjusted using the program *O* v.8.0 (Jones *et al.*, 1991). Elbow angles were obtained by calculating the dot product of the pseudo-dyad axes of the variable and the constant domains. Coordinates of all C^{α} atoms were used in this calculation, which was performed using *CNS*. Calculation of buried surface areas was performed in *X-PLOR* using a 1.6 Å probe. They were determined by subtracting the accessible surface areas of each domain taken as a single BJ dimer and as a BJ dimer in the presence of crystallographic neighbours. Torsion-angle analysis of the final models was based on *PROCHECK* (Laskowski *et al.*, 1993) from the *CCP*4 program suite. Figures were generated using *PyMOL* (DeLano, 2002).

3. Results

The amino-acid sequence of BJ KWR as determined by conventional protein-sequencing methods is presented in Fig. 1. The corresponding CDR loop regions are highlighted. This protein belongs to the immunoglobulin λ light chains of subgroup II. Its amino-terminal residue is a pyroglutamic acid. There is an interchain disulfide bridge between cysteines at amino-acid position 216, which makes this protein a covalently bound homodimer of 45 379 Da. Mass spectrometry showed

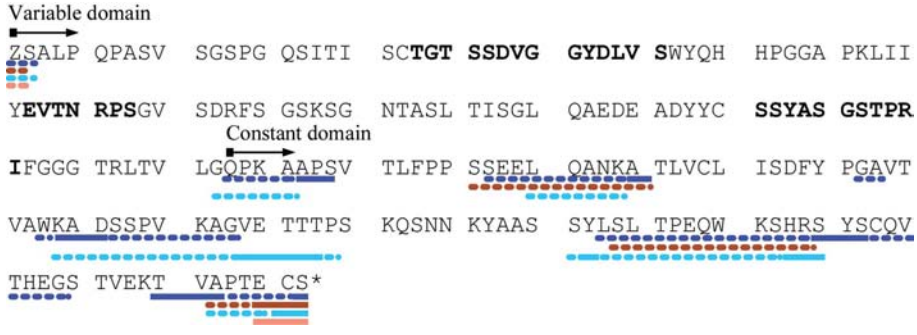

Figure 1
Disordered regions of molecules in the $P3_121$ crystal. Sequences underlined with full lines represent regions of the BJ KWR model in which no density was found in $2F_o - F_c$ maps. The dashed lines indicate weak density. Disordered regions in chains *A*, *B*, *C* and *D* are indicated in pink, light blue, brown and dark blue, respectively. Residues in bold correspond to the CDRs.

that the protein is not glycolsylated and the theoretical pI was calculated to be 6.09 using *ProtParam* (Bjellqvist *et al.*, 1994).

3.1. $P3_121$ crystal form

This was the first of four structures to be determined. In almost every way it was the most difficult to solve, but in many ways it was the most illuminating in terms of its biological implications. The crystals were only observed once and then only after more than eight months of standing at room temperature. As noted previously, such a lag time is almost invariably a consequence of proteolytic cleavage and degradation arising from microbial contamination (McPherson *et al.*, 2004; McPherson, 1999). Because of insufficient remaining material in the crystallization sample, however, this could not be confirmed by gel electrophoresis or mass spectrometry. Calculation of V_M (3.52 Å^3 Da^{-1}) indicated the crystals to have two entire BJ KWR dimers as the asymmetric unit. However, given the likelihood of proteolysis it could not be assumed that the molecules were completely intact. Thus, the precise nature of the asymmetric unit was ambiguous throughout the structure determination.

When a search was conducted with BJ MCG (from PDB entry 1dcl; Ely *et al.*, 1989) using variable elbow angles, a convincing solution was found with elbow angles of 123–143° and 223–238°, which are in fact equivalent. The rotation solutions for both molecules in the asymmetric unit had the same orientation and they were related by a translation of almost exactly one half along the *c* axis. Examination of a native Patterson map showed the presence of a very strong non-Harker peak at (0, 0, 1/2) having a height of 49.7% of the origin peak, consistent with the molecular-replacement solution. Rigid-body refinement of the two dimers comprising the model and further adjustment of the elbow angles produced a conventional *R* factor of 42.8% at 15–2.8 Å with a 4.0σ cutoff on the data.

A significant improvement in the refinement statistics was only achieved when isotropic *B* values of individual atoms were refined. Certain regions of the model, which were apparently subject to disorder, converged to values well in excess of 100 Å^2. These regions were almost exclusively in corresponding sections of the constant domains of the two dimers comprising the asymmetric unit. Calculation and examination of $2F_o - F_c$ and $F_o - F_c$ difference Fourier maps showed the regions indicated by high *B* factors to be occupied by very weak density, which in some cases was wholly absent. This suggested that these regions were likely to be disordered owing to proteolysis and were possibly entirely absent from the constant domains. The variable domains of both dimers within the asymmetric unit, on the other hand, were well resolved. It was evident at this point, particularly given the history of the crystals, that proteolytic cleavage of the BJ KWR had indeed occurred and that the $P3_121$ crystals were in fact composed of degraded protein molecules. Residues for these regions were nonetheless built using low contour levels in the electron-density maps and they were included in subsequent rounds of refinement with high *B* values. Ultimately, the refinement converged to an *R* value of 23.5% and an R_{free} of 28.4%, using all data within 40–2.9 Å resolution. Additional statistics are presented in Table 2.

Fig. 2 shows both molecules in the $P3_121$ asymmetric unit; residues having *B* factors higher than 95.0 Å^2 are indicated in red. The individual polypeptide chains of molecule 1 are designated chains *A* and *B* and those of molecule 2 chains *C* and *D*. The disordered and possibly missing segments of these chains are almost entirely in the constant domains, principally the *B* and *D* chains.

The BJ KWR sequence shown in Fig. 1 indicates those segments in which either no density or spurious electron density was observed. As seen in Figs. 1 and 2, the severity of disorder is greater for molecule 2. The elbow angle is also greater for molecule 2 than for molecule 1 by 2.8°. These two factors, which are possibly correlated, are responsible for the presence of two molecules rather than one molecule in the asymmetric unit and for the doubling of the unit-cell volume. The organization of the Bence Jones dimers in these crystals is noteworthy. It has been observed by others that in amyloidogenic BJ proteins the constant domain is more susceptible to degradation than the variable domain (Solomon & McLaughlin, 1969). Furthermore, the packing arrangement of the variable and constant domains in an amyloid fibril most commonly exposes constant domains, thereby making them more susceptible to proteolysis than the less accessible variable domains (Solomon *et al.*, 1998). We noted in passing that the central solvent channel about the unique axis of the $P3_121$ crystals is sufficiently large in

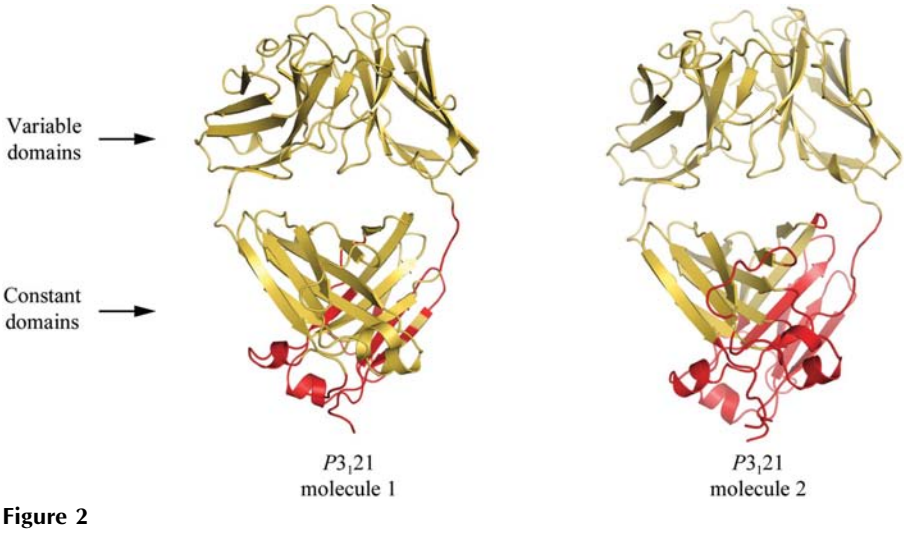

Figure 2
The two BJ KWR molecules in the asymmetric unit of the $P3_121$ crystal. Regions where *B*-factor values exceed 95.0 Å^2 are shown in red.

Table 1
Molecular-replacement solutions obtained using *Phaser* for the orthorhombic data and *CNS* for all other data sets.

	Rotation (Euler) (°)			Translation (orthogonal) (Å)		
Crystal form	θ_1	θ_2	θ_3	x	y	z
$P4_32_12$	64.5	67.1	33.9	14.7	24.8	−94.9
$P2_12_12_1$	184.1	164.1	94.3	55.7	60.8	−14.6
$P3_221$	92.2	74.7	353.8	−36.3	65.2	−37.6
$P3_121$, molecule 1	89.9	74.8	353.8	115.2	63.8	−57.7
$P3_121$, molecule 2	89.5	73.5	354.6	114.3	65.8	−10.7

diameter that smaller proteases such as trypsin could pass along the channel and come into contact with the constant domains of the BJ KWR protein. Thus, it is possible that some proteolysis could have occurred after the crystals had grown. Such a process was also suggested after an *in vivo* analysis of the AL amyloid fibrils by Harris *et al.* (2000). It is unlikely in our experiment, however, that such proteolysis was exclusively the case.

3.2. $P4_32_12$ crystal form

Diffraction data were collected from a single tetragonal crystal of BJ KWR. An initial molecular-replacement probe was derived from the model of the $P3_121$ crystals. The molecular-replacement solution for the tetragonal crystal is presented in Table 1. The tetragonal crystals of BJ KWR provided the highest resolution model, at 2.2 Å. The final conventional R factor is 22.6%, with an $R_{\rm free}$ of 28.3%. Statistics regarding this model, along with others, are shown in Table 2. The model contains all 217 amino-acid residues and 3192 atoms, with average B factors of 58.3 Å^2. It is noteworthy that the B-factor distribution was rather uniform and, other than the last five residues in the C-terminal region, no strikingly high values were observed. SDS–PAGE of the tetragonal crystals confirmed that they were indeed composed of intact BJ dimers.

In addition to the protein and solvent atoms, the model also included three ions, presumably sulfate given the crystallization conditions. In addition, we found a tightly bound molecule, the origin of which is at best obscure, but that was present in all crystal forms (see below) and was modeled as a phenol group. Analysis of a Ramachandran plot showed 98.6% of the amino-acid torsion angles to be in the most favored regions and 1.1% to be in disallowed regions. Among the latter were amino-acid residues *A*28 (Asp), *A*53 (Val), *B*53 (Val), *A*156 (Asp) and *B*214 (Thr). The first two residues belong to CDR loops 1 and 2 and were also found to be in disallowed regions in the other crystal forms, as well as in other λ-type light-chain dimers (Furey *et al.*, 1983; Ely *et al.*, 1989; Huang, Ainsworth, Stevens *et al.*, 1996; Terzyan *et al.*, 2003). Torsional strain is possibly the cause of these frequent outliers, since they are involved in tight β-type (CDR-1) and γ-type (CDR-2) turns. The elbow angle relating the constant and variable domains was 125.8°, which differs from the starting model BJ MCG by 13.5°. The tetragonal crystals had a relatively low solvent content of 45.8%, which was reflected in a tight packing of molecules in the lattice as illustrated in Fig. 3.

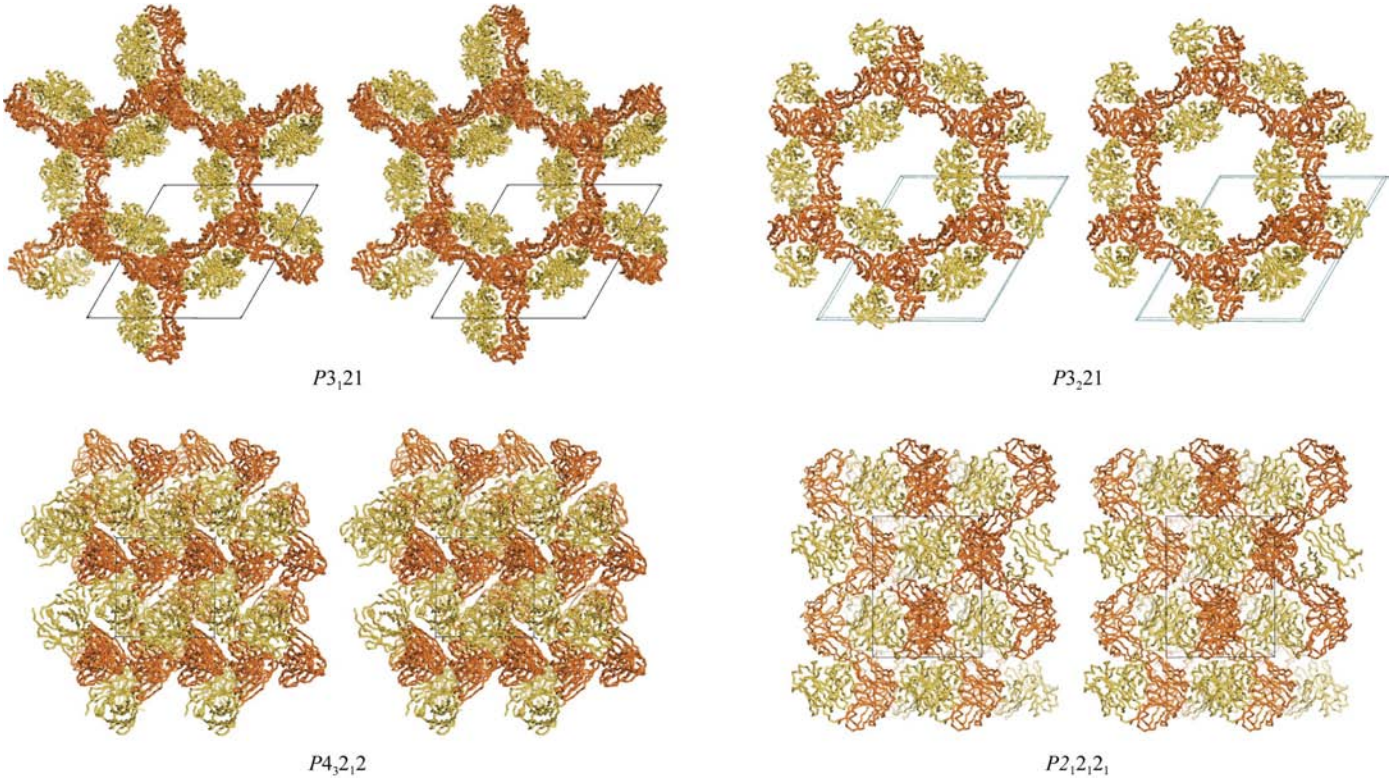

Figure 3
Stereo diagrams of the packing of BJ KWR protein in all four space groups. The variable and constant domains are indicated in orange and yellow, respectively.

3.3. $P2_12_12_1$ crystal form

Orthorhombic crystals were frequently seen to nucleate and grow from the surfaces of tetragonal crystals in the mother liquor and occasionally the two crystal forms interpenetrated as orthorhombic blades grew 'through' the tetragonal blocks (Makino *et al.*, 2005). A close examination of crystal packing shows that the arrangement of molecules in the *ab* planes of the orthorhombic and tetragonal crystals are almost identical to one another, but the absence of diagonal twofold-symmetry axes in the orthorhombic crystals results in different packing of molecules along the *c* direction. The process of orthorhombic crystals growing from the (110) planes of tetragonal crystals represents another interesting case of epitaxic nucleation of one crystal form upon another (McPherson & Shlichta, 1988), rather than the perversion of one crystal lattice to create a second.

Many of the orthorhombic crystals we examined showed signs of disorder, twinning or failure to diffract to high resolution or were afflicted with other problems. Because the structure of BJ KWR had been established in the $P4_32_12$ and $P3_221$ crystal forms, detailed refinement of this crystal was not pursued. The orientation and position of the molecules were determined by molecular replacement using the model from the tetragonal crystals and are presented in Table 1. Rigid-body refinement followed by cycles of Powell minimization, simulated annealing and *B*-factor refinement, but with no model adjustment otherwise or inclusion of any nonprotein atoms, yielded a conventional *R* factor of 26.2% and $R_{\rm free}$ of 35.3% at 3 Å.

3.4. $P3_221$ crystal form

The refined model from the tetragonal crystal was used as probe in a molecular-replacement search of the $P3_221$ crystals, which were grown at pH 4.0 from sodium/potassium phosphate. The rotation and translation parameters relating the orientation and position of the molecules in the two crystal forms are shown in Table 1. It is noteworthy that identical rotation solutions are observed in both trigonal crystal forms and that the difference in the *z* coordinates of molecules 1 and 2 of $P3_121$ crystal equals the *c* axis length of the $P3_221$ cell. The model of the protein in the $P3_221$ crystal was refined as for the tetragonal form but to 2.6 Å resolution. The conventional *R* factor was 21.5%, with an $R_{\rm free}$ of 25.4%. Other relevant statistics are provided in Table 2. In these crystals, 66 ordered water molecules were included, although the overall solvent content (64.6%) is considerably greater than for the tetragonal form. Six ions were observed, presumably phosphates from the mother liquor. Again, a phenol molecule was used to model the unexplained ligand (see below).

In both trigonal crystals, the molecules are arranged in a helical fashion about a large solvent channel of about 84 Å in diameter coincident with the threefold screw axis, as illustrated in Fig. 3. Although the hands of the two trigonal space groups are opposite, as further described in Fig. 4, the packing of molecules about the central channel along the unique direction is virtually identical. The hand of the helices of protein molecules is a right-handed double helix with 12 BJ KWR per turn in both cases. The *B* values for the residues in the constant domains of the BJ KWR in the $P3_221$ crystals are again quite high, which in turn affects the quality of the electron density. However, unlike these residues in the $P3_121$ trigonal form, in which large regions of backbone were completely absent, in the $P3_221$ crystal this is not so: virtually all residues are present and are represented as a contiguous chain in electron-density maps. Indeed, SDS–PAGE shows that the $P3_221$ crystals, which grow at low pH and in only a few days, are composed of completely intact molecules. Thus, it appears that when the constant domains are not constrained by significant lattice interactions, as they are in the tetragonal

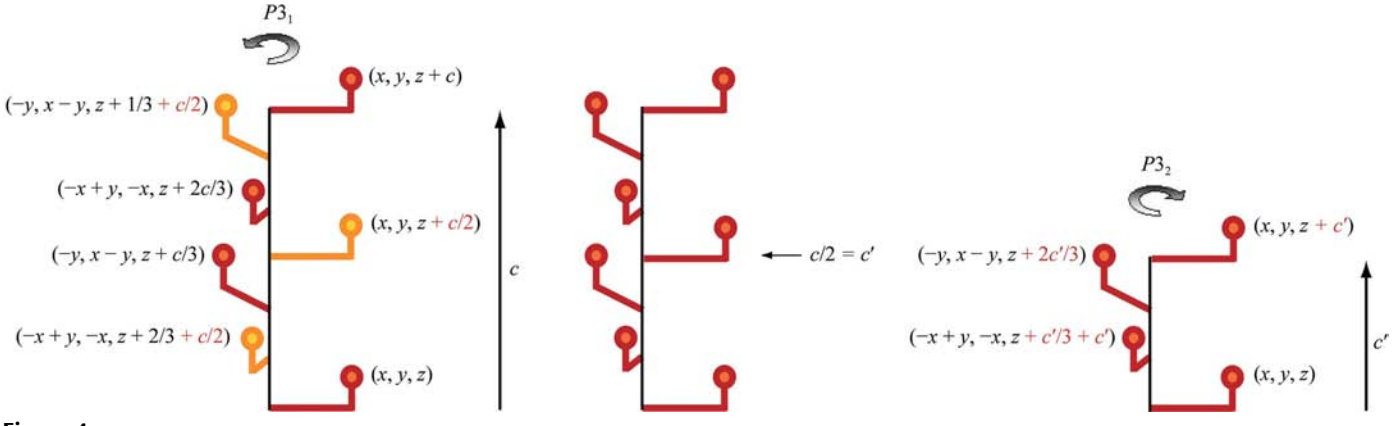

Figure 4
Diagram illustrating the transformation in space-group handedness when two unique molecules in the asymmetric unit separated by *c*/2 become identical. Molecule 1 is represented in red and located at general position (*x*, *y*, *z*) in the $P3_1$ cell of axis length *c*, shown on the left. Molecule 2, which is almost identical in conformation and orientation to molecule 1, is at general position (*x*, *y*, *z* + *c*/2) and indicated in yellow. Equivalent molecules about the axis are generated by applying 3_1 symmetry. When molecule 2 is equivalent to molecule 1, we obtain the center diagram in which all molecules are red. The repeat unit along the *c* axis is now $c' = c/2$ and the space group has changed to $P3_2$ with a left-handed screw axis, as shown on the right. However, the packing of the two space groups are exactly the same. Thus, in each space group the molecules form a right-handed double helix with a repeat length of *c*. In space group $P3_121$, the molecules along the helix alternate between molecule 1 and molecule 2, which have quasi-twofold relationships that reduce to exact twofold relationships in space group $P3_221$.

Table 2
Refinement statistics.

Values in parentheses are for the highest resolution shell.

Space group	$P3_121$	$P3_221$	$P4_32_12$
Unit-cell parameters (Å)	$a = b = 153.5$, $c = 94.0$	$a = b = 155.4$, $c = 46.9$	$a = b = 68.6$, $c = 181.7$
Resolution (Å)	40–2.9 (3.0–2.9)	40–2.6 (2.69–2.60)	45–2.2 (2.28–2.20)
σ-Cutoff	0.0	0.0	0.0
No. of reflections in working set	24350 (2136)	17786 (1606)	17773 (946)
No. of reflections in test set	1820 (167)	1943 (183)	1929 (109)
R_{free} (%)	28.4 (37.6)	25.4 (35.7)	28.3 (39.3)
R_{work} (%)	23.5 (34.5)	21.5 (32.0)	22.6 (40.3)
Protein			
Residues	434	217	217
Atoms	6384	3192	3192
Nonprotein atoms			
Water	16	66	98
Ion	45	30	15
Phenol group	14	7	7
R.m.s. deviations			
Bond length (Å)	0.0078	0.0064	0.0068
Bond angles (°)	1.45	1.31	1.44
Average B factor (Å^2)			
Protein	68.2	66.1	58.3
Phenol molecule	51.3	42.2	57.9
Solvent	80.1	60.2	56.3
Chain A, variable	44.7	48.4	54.1
Chain A, constant	60.4	68.9	64.0
Chain B, variable	52.0	42.5	46.9
Chain B, constant	102.2	105.5	68.5
Chain C, variable	40.9	—	—
Chain C, constant	84.6	—	—
Chain D, variable	45.0	—	—
Chain D, constant	112.8	—	—
Ramachandran plot			
Residues in the most favored regions (%)	97.2	98.8	98.6
Residues in generously allowed region (%)	2.1	0.6	0.3
Residues in disallowed region (%)	0.7	0.6	1.1

Table 3
Buried surface area of the variable and constant domains of each crystal form calculated using *X-PLOR* with a 1.6 Å probe.

		Buried surface area (Å^2)			
	Chain	A	B	C	D
$P3_121$	Variable domain	1455	742	1617	762
	Constant domain	986	566	789	344
$P3_221$	Variable domain	1360	724	—	—
	Constant domain	978	284	—	—
$P4_32_12$	Variable domain	836	1364	—	—
	Constant domain	1196	1101	—	—

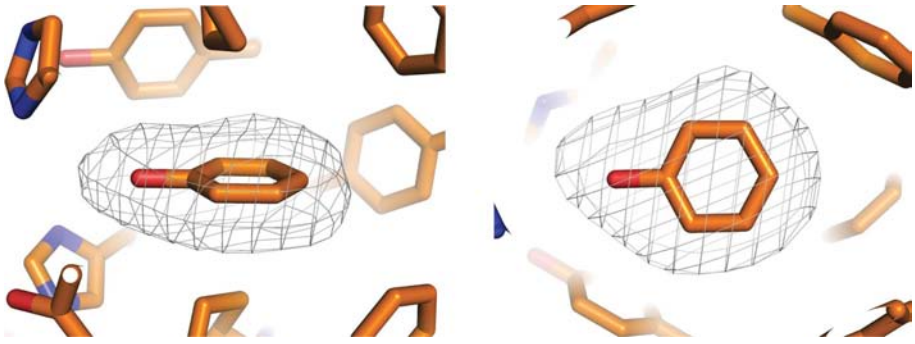

Figure 5
$F_o - F_c$ OMIT map calculated after simulated annealing of the $P3_221$ crystal at 2.6 Å and contoured at a level of 3.0σ. The electron density of the unknown ligand, here represented as a phenol molecule, was found in the 'deep pocket' of BJ KWR.

and orthorhombic crystals, the polypeptide chains comprising the domains and perhaps even the entire domains themselves exhibit an appreciable degree of mobility. Proteolysis apparently enhances the dynamic character of the constant domains even further by introducing additional opportunities for structural flexibility.

In the trigonal crystals, the arrangement of the molecules about the threefold screw axes possesses pseudo-sixfold symmetry and this was especially evident in self-rotation function maps. 12 molecules occupy one turn of a helix and this may have implications for fibril formation, as discussed below. Fig. 3 illustrates the molecular packing of each crystal form, with the variable domains indicated in orange and the constant domains in yellow. The helical structure with a central channel is not present in the tetragonal and orthorhombic crystals and in the trigonal forms the variable domains form most of the framework of this structure. Indeed, as shown in Table 3, a solvent-accessibility calculation using the $P3_121$ model as well as the $P3_221$ and $P4_32_12$ models indicates that the variable domains have significantly greater buried surface area than the constant domains. This feature is exclusive to the trigonal forms, as evidenced by the comparatively large buried surface area of the constant domains of the tetragonal form.

3.5. The unknown ligand

A two-compartment 'antigen'-binding system was first described by Edmundson, Ely *et al.* (1989) for BJ MCG and was further considered as a model for a primitive antibody. This system is comprised of a main cavity, which is formed by the CDR loops in the conventional way, and a deep pocket found beneath the main cavity floor. It was shown that these compartments can be occupied by various ligands (Edmundson, Herron *et al.*, 1989). Such an interior cavity was observed in the same location in BJ KWR. A molecule of unknown origin was unambiguously identified in the deep pocket in all the refined BJ KWR structures. This is illustrated in Fig. 5. A

review of the components of all of the mother liquors used to grow the crystals offered no suggestion as to its nature and we have concluded that it is something from the original preparation of over 40 years ago and may in fact have accompanied the protein from the patient himself. In any case, unable to identify it definitively, we used a molecule of phenol, which seemed to best conform to the density, to model it.

3.6. Bound ions

In all four crystal forms of BJ KWR, ions were observed bound to the protein in the main cavity of the conventional antigen-binding site of a Fab. They are presumably sulfate ions in the $P4_32_12$ and $P3_121$ unit cells and phosphate ions in the second trigonal crystal form. The ions are shown in Fig. 6. The sulfate ions interact most closely with the amino-acid side chains of Tyr38 and Arg100. In the $P3_221$ crystal the sulfate site is occupied by a phosphate group, while a second phosphate is observed within the same region and interacts with residues Tyr38 and Ser36 of another BJ monomer. The second phosphate ion in the $P3_221$ crystal also interacts indirectly with symmetry-related residues Thr206 and Gly204. The two phosphates are disposed in the cavity in such a way that an extensive network of hydrogen bonds involving the ions, water and the protein is created.

In addition to ions bound to the surface of BJ KWR and in the main cavity, additional density, modeled as phosphate, was found near the elbow of the refined model in the $P3_221$ crystal. This ion interacts with Arg*B*107 and the backbone amide of Gly*A*43 and through a water molecule with Asp*A*87 and Tyr*A*89.

3.7. Comparison of models

A comparison was made of the models for the tetragonal, orthorhombic and two trigonal crystals. The elbow angles relating the domains were 125.8° in the tetragonal crystals, 128.9° in the orthorhombic crystals and 132.7° in the $P3_221$ crystal form. The elbow angles for the two molecules in the $P3_121$ crystals were 132.3° and 135.2°. Thus, the KWR homodimer was clearly flexible in this regard over a range of about 10°. We presume that the assumption of these different angles must be a function of the intermolecular interactions within the various crystals or variations arising from differences in the crystallization conditions. Superposition of the variable and constant domains separately, detailed in Table 4, shows that the overall r.m.s. deviation for the constant domains is higher on average than for the variable domains. The last two or three residues at the C-termini were fitted into difference and OMIT map densities contoured at a level of 0.5σ and refined to *B*-factor values of about 130 Å^2. Weak densities for these residues were observed in all crystal forms. No persuasive electron density was found for the interchain disulfide bond located at position 216.

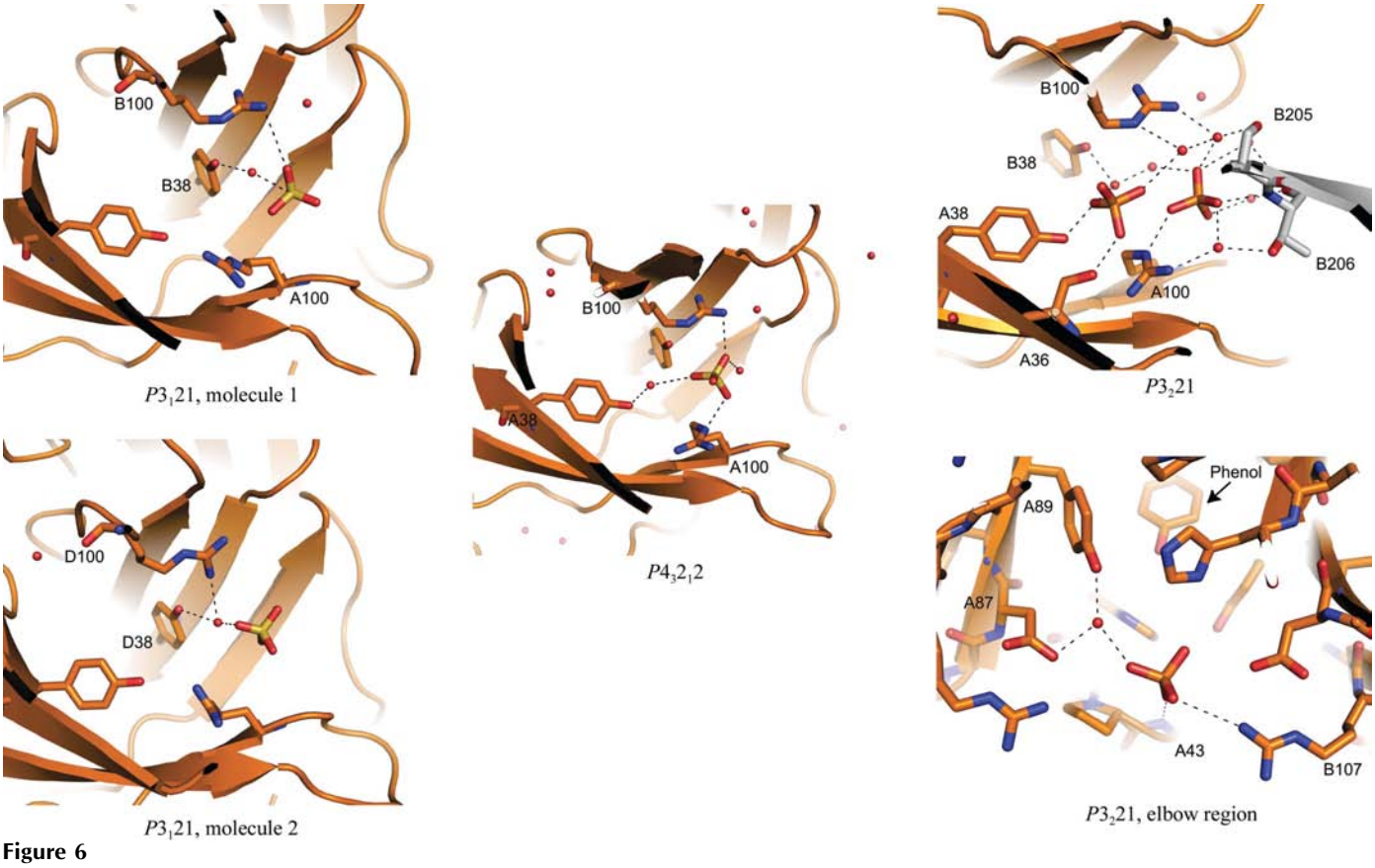

Figure 6
Sulfate-ion and phosphate-ion interactions in the main cavity of what would be the antigen-binding site of a Fab. The elbow region of the $P3_221$ crystal shows the location of the phenol molecule and a phosphate also observed in that region. A symmetry-related molecule is indicated in gray.

Table 4
R.m.s. deviation between variable domains (residues 1–112) and constant domains (residues 113–217) of models from each BJ KWR crystal form.

Main-chain r.m.s.d. values are shown in the upper diagonal. Side-chain r.m.s.d. values are in bold and are shown in the lower diagonal.

	Variable domain				Constant domain			
Space group	$P4_32_12$	$P3_221$	$P3_121$, molecule 1	$P3_121$, molecule 2	$P4_32_12$	$P3_221$	$P3_121$, molecule 1	$P3_121$, molecule 2
$P4_32_12$	—	0.815	0.851	0.841	—	1.109	1.639	1.860
$P3_221$	**1.247**	—	0.476	0.442	**2.066**	—	1.413	1.561
$P3_121$, molecule 1	**1.186**	**0.931**	—	0.473	**2.490**	**2.063**	—	1.929
$P3_121$, molecule 2	**1.286**	**1.009**	**0.935**	—	**2.799**	**2.333**	**2.596**	—

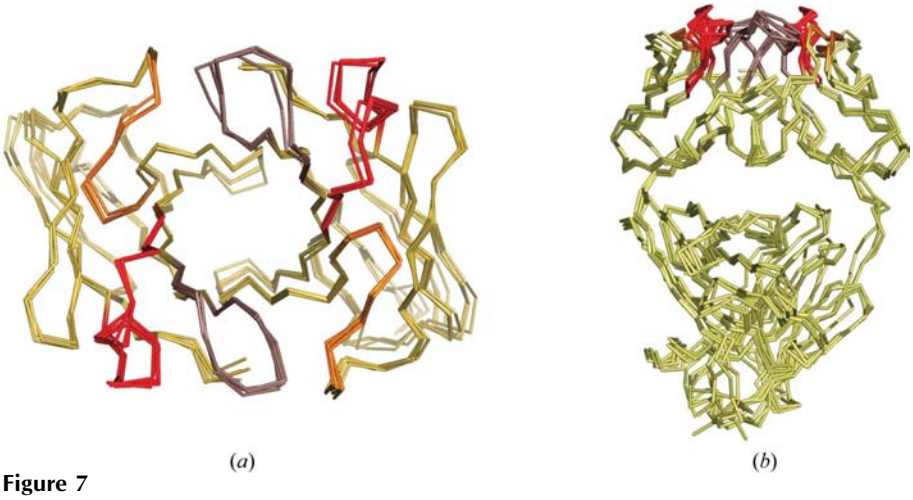

Figure 7
(*a*) Backbone superposition of variable-domain models for the $P3_121$, $P3_221$ and $P4_32_12$ crystal forms. The CDR-1 loop is highlighted in red, the CDR-2 loop in orange and the CDR-3 loop in brown. R.m.s.d. values between variable domains for main-chain atoms only range between 0.50 and 0.88 Å. (*b*) Full-length light-chain dimer superposition showing the CDR region and the blunt topography of the BJ KWR antigen-combining site.

The CDR loops are well ordered in all models and there was no ambiguity in identifying the backbone and side-chain atoms in the electron density. Superposition of the variable domains of all refined models indicates that the CDR conformations within the trigonal models are the same within experimental error, with r.m.s.d. values that range between 0.50 and 0.88 Å. The tetragonal model has its CDR loops slightly displaced with respect to the trigonal models, as might be expected from the different crystal-packing arrangements. Fig. 7(*a*) shows the backbone superposition of the variable domains and the CDR loops of the tetragonal and the two trigonal models.

We analyzed the CDR-loop conformations in the models refined at higher resolution, *i.e.* from the $P4_32_12$ and $P3_221$ crystals. The loops were compared with canonical three-dimensional structures of λ-type light-chain CDRs (Al-Lazikani *et al.*, 1997). In both models, CDR-1 shows the three characteristic hydrogen-bond interactions found in the λL1 canonical class 2, as described in Al-Lazikani *et al.* (1997). In BJ KWR, these are between the carbonyl O atom of Thr25 and the amino N atoms of Asp28 and Gly30 and between the carbonyl O atom of Asp28 and the amino N atom of Gly31. An additional hydrogen bond was found between the carbonyl O atom of Asp28 and the amino N atom of Tyr32. The CDR-2 of BJ KWR also conforms to the canonical hairpin loop, which adopts a classic γ-turn with average dihedral angles for the residue at the turn, Val53, of $\varphi = 69.4^\circ$ and $\psi = -49.8^\circ$ for the $P4_32_12$ model and $\varphi = 62.6^\circ$ and $\psi = -56.2^\circ$ for the $P3_221$ model. The third CDR loop of BJ KWR does not seem to adopt a canonical disposition. The presence of Pro99 at the beginning of the turn may preclude any of the hydrogen-bond patterns found in canonical λL3 loops.

Fig. 7(*b*) is a view of BJ KWR in which the planar topography of the CDRs can be readily observed. There is no knowledge of the particular antigen that this light chain binds when associated with its corresponding heavy chain. However, a complete analysis of Fab topographies (MacCallum *et al.*, 1996) indicates that a combining site lacking strong topographical features is most characteristic of antibodies which bind protein antigens.

4. Discussion

Different theories exist concerning the fibrilogenesis of BJ proteins. One theory, for example, is that specific subclasses of immunoglobulin light chains (Stone, 1990) exhibiting particular amino-acid mutations or insertions (Alim *et al.*, 1999; Glenner, Terry *et al.*, 1971) would be more amyloidogenic than others. What does appear to be certain, however, is that AL-type amyloid fibrils are generally derived from fragments of monoclonal light chains and rarely from complete chains (Glenner, 1980). While the mechanism of AL-type amyloid formation has not been established, considerable evidence suggests that proteolysis of full-length light chains is a principal mechanism for the formation of amyloid fibrils (Linke, Zucker-Franklin *et al.*, 1973). It has been shown, for example, that soluble BJ proteins form amyloid fibrils *in vitro* as a result of proteolysis (Glenner, Ein *et al.*, 1971; Linke, Tischendorf *et al.*, 1973; Wall *et al.*, 1999). Several proteases produce this effect, including trypsin, pepsin and kidney lysosomal enzymes (Epstein *et al.*, 1974).

There are several lines of evidence suggesting that the helical arrangement of BJ KWR observed in the trigonal crystals analyzed here may reflect the structure assumed by BJ proteins when they form fibrils characteristic of deposition diseases. First of all, it is known that fibril formation frequently involves proteolytically modified or degraded fragments of BJ proteins. The degradation is normally confined to the constant domains of the proteins and fibril formation is then mediated through intermolecular interactions involving mainly or only the variable domains. In three different crystal forms of BJ KWR the protein was intact. However, the molecules in the $P3_121$ crystals were degraded exclusively in the constant domains, formed hollow double-helical structures based on pseudo-sixfold screw symmetry and exhibited a counter-clockwise handedness. As described below, these features are consistent with the amyloidogenic BJ BRE fibril model, which is composed solely of variable domains (Schormann *et al.*, 1995; Steinrauf *et al.*, 1999).

The $P3_221$ crystals also form the helical arrangement seen in the $P3_121$ crystals, but are composed of intact BJ proteins. The former, however, were grown at very low pH and, significantly, this is the second mechanism suggested to promote amyloid-fibril formation. Experiments by Khurana *et al.* (2001) demonstrated that AL amyloid fibrils or amorphous aggregates appear from intermediate protein-folding states induced by acidic pH. Thus, the two crystals of the four studied here whose packing arrangements were based on large open channels with pseudo-sixfold symmetry both involved one of the two factors known to induce amyloid-fibril formation.

Secondly, there is the appearance of the unknown ligand, which we have modeled as a phenol molecule, in the so-called 'deep pocket' below the antigen-binding site. Studies have been carried out on the binding of various small-molecule non-antigen ligands to BJ proteins by other investigators (Edmundson, Herron *et al.*, 1989). In a study of BJ MCG (Edmundson, Ely *et al.*, 1989), the BJ protein of highest homology to BJ KWR and that which served as the initial probe for our molecular-replacement solution, it was shown that bis(dinitrophenyl)lysine was tightly bound to BJ MCG in the same deep pocket in which we identified a bound ligand in BJ KWR. This is significant because another report states that the binding of the ε-(dinitrophenyl)lysine group only occurred for the BJ proteins of patients whose multiple myeloma was accompanied by amyloidosis (Bertram *et al.*, 1980).

Thirdly, the variable domains responsible for the formation of the helical arrangement in the trigonal crystals use a pattern of intermolecular interactions which is not seen in the other crystal forms of BJ KWR or in crystals of most other BJ proteins. An extended β-pleated antiparallel sheet has frequently been proposed to be a distinctive bonding motif in amyloid fibrils (Glenner, 1980). As shown in Fig. 8(*a*), a lateral interaction is formed involving a network of four hydrogen bonds between the outside strands of antiparallel β-sheets on neighboring molecules. This lateral interaction has pseudo-twofold symmetry similar to that observed in other types of amyloid-fibril models (Serag *et al.*, 2002; Elam *et al.*, 2003). Residues 11–13 in both molecules contribute to this interaction. An extended antiparallel β-sheet joining two molecules is thereby created. A similar hydrogen-bonding network is also found in the amyloidogenic BJ BRE model (Schormann *et al.*, 1995; Steinrauf *et al.*, 1999). In the BJ BRE network, three hydrogen bonds form an extended β-sheet involving a sequence corresponding to that in BJ KWR. The opposite side of the variable domains of BJ KWR, seen in Fig. 8(*b*), interacts through a single hydrogen bond between an unstructured extended loop and a β-strand from a symmetry-related variable domain. The residues involved in this hydrogen bond are Ser*A*9 and Asp*C*55. The percentage of

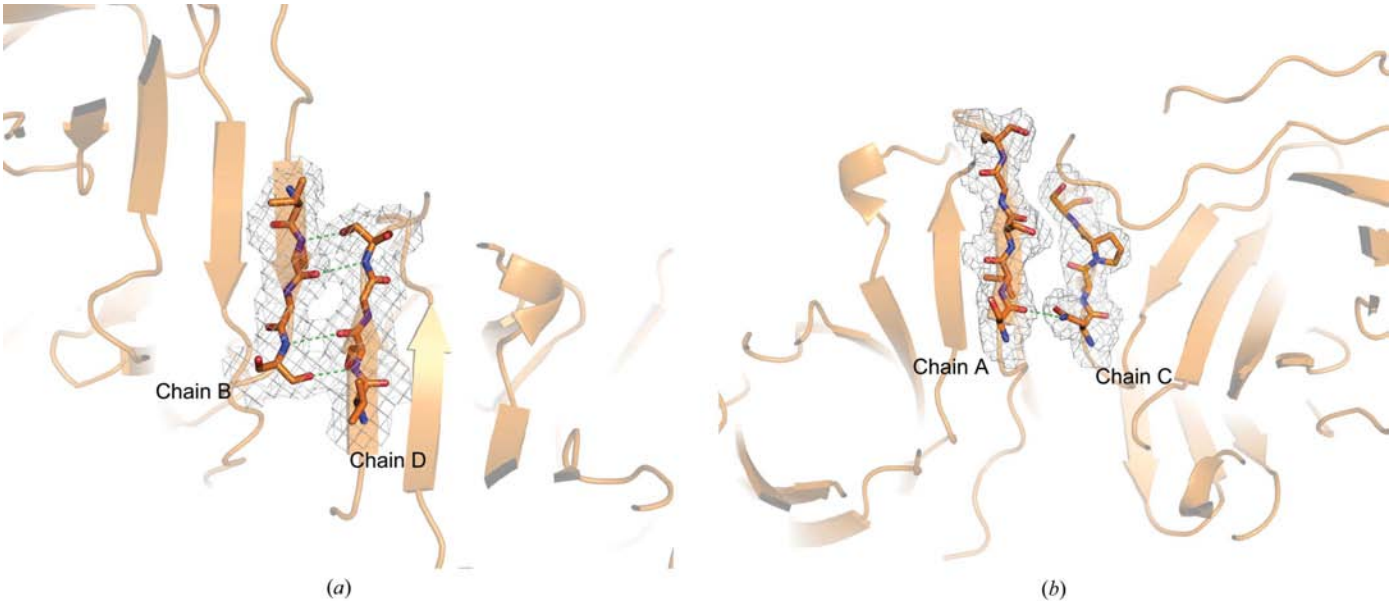

Figure 8
Detail of the lateral interactions between neighboring variable domains in the $P3_121$ crystal. (*a*) Interaction between adjacent β-strands from two variable domains of chains *B* and *D* forms an extended β-sheet; (*b*) lateral interactions between neighboring variable domains of chains *A* and *C*.

the surface participating in this type of interaction was calculated using *X-PLOR*. This was obtained by dividing the solvent buried area by the total solvent-accessible surface area of independent variable domains. On average, 6.7% of the variable-domain surface participates in interactions between variable domains of chains *B* and *D* as seen in Fig. 8(*a*) and 7.7% contributes to the interaction of variable domains of chains *A* and symmetry-related chains *C* as seen in Fig. 8(*b*).

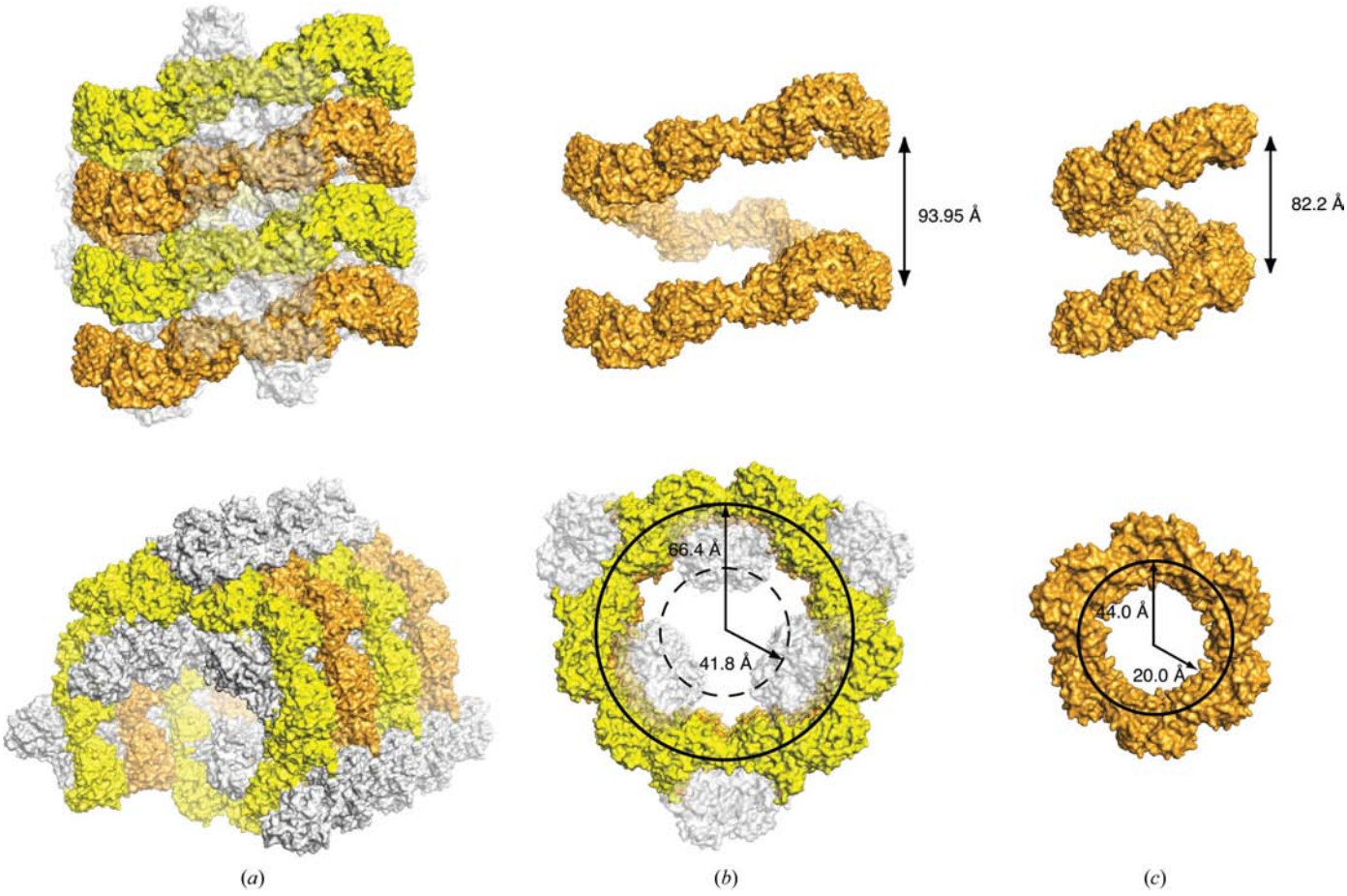

Figure 9
Comparison between the helical structure of BJ KWR, as found in the crystal, and an AL-type amyloid-fibril model of BJ BRE. (*a*) The BJ KWR double helix found in the trigonal crystal is highlighted in yellow and orange and the constant domains are shown in gray. A single helix was extracted from (*a*) and is shown in (*b*) without the constant domains. This constitutes a right-handed helix of 93.95 Å height and with an average radius of 66.4 Å. BJ BRE also forms a right-handed helix and is illustrated in (*c*). The calculated height of BJ BRE is 82.2 Å, with an average radius of 44 Å.

Figure 10
Three crystallographically adjacent BJ proteins in the crystals of BJ KWR (*a*) and BJ BRE (*b*) are shown in schematic representation with the variable domains highlighted in orange. The packing corresponds to that in the $P3_121$ crystals for BJ KWR and the $P2_1$ unit cell for BJ BRE. Numbers indicate individual dimers.

Finally, examination of the pseudo-sixfold helical arrangement of BJ KWR in the trigonal crystals shows it to be compatible with current proposals for the structure of amyloid fibrils. An amyloid-fibril model based on the crystallographic packing of the amyloidogenic BJ BRE has been proposed which was formulated based only on the variable domains of a κ I light-chain dimer (Schormann *et al.*, 1995; Steinrauf *et al.*, 1999). The crystals in this case were monoclinic, but the BJ BRE variable domains arranged themselves in the form of a pseudo-sixfold helix to form a hollow cylinder of 115 Å diameter, as described in Schormann *et al.* (1995) and in Steinrauf *et al.* (1999).

Fig. 9(*a*) shows surface representations of the BJ KWR helical duplex observed in the trigonal crystals in two different orientations, shown at the top and bottom of the figure. One single helical fibril is presented in Fig. 9(*b*) without the constant domains. The proposed fibril structure of BJ BRE derived from a monoclinic crystal is presented in Fig. 9(*c*). Both have the same hand, but differ significantly in pitch and diameter. The pitch of the BJ KWR helix is 94 Å, while that for BJ BRE is about 78 Å. The average diameter of the BJ KWR fibril is 133 Å and that of its solvent channel is 84 Å, both of which are about 40 Å greater than those in the BJ BRE model. The differences in pitch and more importantly diameter are undoubtedly explained by the components of the two helices. The BJ BRE fibril model is composed exclusively of the variable domains of the BJ dimers, while the fibrils of BJ KWR are composed of molecules possessing intact, disordered or partially degraded constant domains. In both the BJ KWR and BJ BRE fibrils, the helix is propagated in a similar manner through hydrogen-bonding interactions involving the variable domains. In the BJ KWR helices, however, the pitch and diameter of the helices are necessarily greater to accommodate interactions between constant domains, which protrude into the central channel.

Fig. 10 provides a view in schematic representation of the crystallographic interactions between three consecutive BJ KWR molecules in the pseudo-sixfold helix along *c*. In Fig. 10(*a*), the variable domains of molecules 1 and 2 interact in a manner very similar to that of BJ BRE molecules 1 and 2, shown in Fig. 10(*b*), by a pseudo-twofold axis. The CDR loops are directed away from the center of the fibril. Because of the presence of the constant domain, albeit in a diminished form, molecule 3 in BJ KWR cannot adopt the same conformation as molecule 3 in the crystals of BJ BRE. Therefore, molecule 3 in BJ KWR has its orientation inverted, so that the CDR loops now point towards the center, thus precluding steric hindrance with adjacent constant domains. The lateral interaction between the variable domains follows the threefold screw axis. In general, the helical structure seen here for BJ KWR is also in reasonable agreement with other observations and data regarding amyloid fibrils formed by degraded immunoglobulin light chains. Thus, we would suggest that the helical structure of BJ KWR seen here in the trigonal crystal forms may indeed be relevant to the formation of amyloid fibrils in general.

We also noted that the CDR loops in BJ KWR were uniformly the same in all copies of the protein in all crystal forms; thus, the quasi antigen-binding region appeared to be rigid and well ordered. The finding of two phosphate or sulfate ions in this site suggests that electrostatic interactions would probably be important in binding the intended antigen. The site overall is rather blunt, without either a deep invagination or a deep channel, suggesting that the natural antigen is probably a protein or polypeptide (MacCallum *et al.*, 1996). The presence of the unknown ligand in the 'deep pocket' is intriguing, but remains a 40-year mystery.

DLM was supported by the Conselho Nacional de Desenvolvimento Científico e Tecnológico (CNPq, Brazil).

References

Alim, M. A., Yamaki, S., Hossain, M. S., Takeda, K., Yamagata, F., Takashi, I. & Shinoda, T. (1999). *Clin. Immunol.* **90**, 399–403.

Al-Lazikani, B., Lesk, A. M. & Chothia, C. (1997). *J. Mol. Biol.* **273**, 927–948.

Barton, G. J. (1990). *Methods Enzymol.* **183**, 403–428.

Berman, H. M., Westbrook, J., Feng, Z., Gilliland, G., Bhat, T. N., Weissig, H., Shindyalov, I. N. & Bourne, P. E. (2000). *Nucleic Acids Res.* **28**, 235–242.

Bertram, J., Gualtieri, R. J. & Osserman, E. F. (1980). *Amyloid and Amyloidosis*, edited by G. G. Glenner, P. P. Costa & F. Freitas, pp. 351–360. Amsterdam: Excerpta Medica.

Bjellqvist, B., Basse, B., Olsen, E. & Celis, J. E. (1994). *Electrophoresis*, **15**, 529–539.

Bourne, P. C., Ramsland, P. A., Shan, L., Fan, Z.-C., Dewitt, C. R., Shultz, B. B., Terzyan, S. S., Moomaw, C. R., Slaughter, C. A., Guddat, L. W. & Edmundson, A. B. (2002). *Acta Cryst.* D**58**, 815–823.

Brünger, A. T. (1992). *X-PLOR. A System for X-ray Crystallography and NMR*, v.3.1. New Haven, CT, USA: Yale University.

Brünger, A. T., Adams, P. D., Clore, G. M., DeLano, W. L., Gros, P., Grosse-Kunstleve, R. W., Jiang, J.-S., Kuszewski, J., Nilges, M., Pannu, N. S., Read, R. J., Rice, L. M., Simonson, T. & Warren, G. L. (1998). *Acta Cryst.* D**54**, 905–921.

Buxbaum, J. (1992). *Hematol. Oncol. Clin. North Am.* **6**, 323–346.

Caputo, C. B. & Salama, A. I. (1989). *Neurobiol. Aging*, **10**, 451–461.

Clamp, J. R. (1967). *Lancet*, **2**, 1354–1356.

Collaborative Computational Project, Number 4 (1994). *Acta Cryst.* D**50**, 760–763.

DeLano, W. L. (2002). *The PyMOL Molecular Graphics System.* DeLano Scientific, San Carlos, CA, USA.

Edmundson, A. B., Ely, K. R., He, X.-M. & Herron, J. N. (1989). *Mol. Immunol.* **26**, 207–220.

Edmundson, A. B., Herron, J. N., Ely, K. R., He, X.-M., Harris, D. L. & Voss, E. W. Jr (1989). *Philos. Trans. R. Soc. Lond., B, Biol. Sci.* **323**, 495–509.

Elam, J. S., Taylor, A. B., Strange, R., Antonyuk, S., Doucette, P. A., Rodriguez, J. A, Hasnain, S. S., Hayward, L. J., Valentine, J. S., Yeates, T. O. & Hart, P. J. (2003). *Nature Struct. Biol.* **10**, 461–467.

Ely, K. R., Herron, J. N., Harker, M. & Edmundson, A. B. (1989). *J. Mol. Biol.* **210**, 601–615.

Epp, O., Lattman, E. E., Schiffer, M., Huber, R. & Palm, W. (1975). *Biochemistry*, **14**, 4943–4952.

Epstein, W. V., Tan, M. & Wood, I. S. (1974). *J. Lab. Clin. Med.* **84**, 107–110.

Furey, W. Jr, Wang, B.-C., Yoo, C. S. & Sax, M. (1983). *J. Mol. Biol.* **167**, 661–692.

Glenner, G. G. (1980). *N. Engl. J. Med.* **302**, 1283–1292.

Glenner, G. G., Ein, D., Eanes, E. D., Bladen, H. A., Terry, W. & Page, D. L. (1971). *Science*, **174**, 712–714.

Glenner, G. G., Terry, W., Harada, M., Isersky, C. & Page, D. (1971). *Science*, **172**, 1150–1151.
Harris, D. L., King, E., Ramsland, P. A. & Edmundson, A. B. (2000). *J. Mol. Recognit.* **13**,198–212.
Henikoff, S. & Henikoff, J. G. (1992). *Proc. Natl Acad. Sci. USA*, **89**, 10915–10919.
Huang, D. B., Ainsworth, C., Solomon, A. & Schiffer, M. (1996). *Acta Cryst.* D**52**, 1058–1066.
Huang, D. B., Ainsworth, C. F., Stevens, F. J. & Schiffer, M. (1996). *Proc. Natl Acad. Sci. USA*, **93**, 7017–7021.
Huang, D. B., Chang, C. H., Ainsworth, C., Brünger, A. T., Eulitz, M., Solomon, A., Stevens, F. J. & Schiffer, M. (1994). *Biochemistry*, **33**, 14848–14857.
Jones, T. A., Zou, J.-Y., Cowan, S. W. & Kjeldgaard, M. (1991). *Acta Cryst.* A**47**, 110–119.
Khurana, R., Gillespie, J. R., Talapatra, A., Minert, L. J., Ionescu-Zanetti, C., Millett, I. & Fink, A. L. (2001). *Biochemistry*, **40**, 3525–3535.
Kintner, M. & Sherman, N. E. (2000). *Protein Sequencing and Identification Using Tandem Mass Spectrometry.* New York: John Wiley.
Krieglestein, K., Henschen, A., Weller, U. & Habermann, E. (1990). *Eur. J. Biochem.* **188**, 39–45.
Laskowski, R. A., MacArthur, M. W., Moss, D. S. & Thornton, J. M. (1993). *J. Appl. Cryst.* **26**, 283–291.
Levinson, S. S. & Keren, D. F. (1994). *Clin. Chem.* **40**, 1869–1878.
Linke, R. P., Tischendorf, F. W., Zucker-Franklin, D. & Franklin, E. C. (1973). *J. Immunol.* **111**, 24–26.
Linke, R. P., Zucker-Franklin, D. & Franklin, E. C. (1973). *J. Immunol.* **111**, 10–23.
Lottspeich, F. & Henschen, A. (1977). *Hoppe-Seyler's Z. Physiol. Chem.* **358**, 1521–1524.
Lounes, K. C., Lefkowitz, J. B., Henschen-Edman, A. H., Coates, A. I., Hantgan, R. R. & Lord, S. T. (2001). *Blood*, **98**, 661–666.
MacCallum, R. M., Martin, A. C. R. & Thornton, J. M. (1996). *J. Mol. Biol.* **262**, 732–745.
McPherson, A. (1999). *Crystallization of Biological Macromolecules.* New York: Cold Spring Harbor Laboratory Press.
McPherson, A., Day, J. & Harris, L. J. (2004). *Acta Cryst.* D**60**, 872–877.
McPherson, A. & Shlichta, P. (1988). *Science*, **239**, 385–387.
Makino, D. L., Henschen-Edman, A. H. & McPherson, A. (2005). *Acta Cryst.* F**61**, 79–82.
Otwinowski, Z. & Minor, W. (1997). *Methods Enzymol.* **276**, 307–326.
Pflugrath, J. W. (1999). *Acta Cryst.* D**55**, 1718–1725.
Plomp, M., McPherson, A. & Malkin, A. J. (2003). *Proteins*, **50**, 486–495.
Read, R. J. (2001). *Acta Cryst.* D**57**, 1373–1382.
Roussel, A., Spinelli, S., Deret, S., Navaza, J., Aucouturier, P. & Cambillau, C. (1999). *Eur. J. Biochem.* **260**, 192–199.
Rossmann, M. G. (1990). *Acta Cryst.* A**46**, 73–82.
Sanders, P. W. (1994). *J. Lab. Clin. Med.* **124**, 484–488.
Schormann, N., Murrell, R. J., Liepnieks, J. J. & Benson, M. D. (1995). *Proc. Natl Acad. Sci. USA*, **92**, 9490–9494.
Serag, A. A., Altenbach, C., Gingery, M., Hubbell, W. L. & Yeates, T. O. (2002). *Nature Struct. Biol.* **9**, 734–739.
Solomon, A. (1986). *Blood*, **68**, 603–610.
Solomon, A. & McLaughlin, C. L. (1969). *J. Biol. Chem.* **244**, 3393–3404.
Solomon, A., Weiss, D. T., Murphy, C. L., Hrncic, R., Wall, J. S. & Schell, M. (1998). *Proc. Natl Acad. Sci. USA*, **95**, 9547–9551.
Steinrauf, L. K., Chiang, M. Y. & Shiuan, D. (1999). *J. Biochem.* **125**, 422–429.
Stevens, F. J. & Myatt, E. A. (1991). *Nanotechnology*, **2**, 206–213.
Stone, M. J. (1990). *Blood*, **75**, 531–545.
Storoni, L. C., McCoy, A. J. & Read, R. J. (2004). *Acta Cryst.* D**60**, 432–438.
Terzyan, S. S., DeWitt, C. R., Ramsland, P. A., Bourne, P. C. & Edmundson, A. B. (2003). *J. Mol. Recognit.* **165**, 83–90.
Wall, J., Murphy, C. L. & Solomon, A. (1999). *Methods Enzymol.* **309**, 204–217.
Wetzel, R. (2002). *Structure*, **10**, 1031–1036.